High Aspect Ratio Cantilever Tips for Non-Contact Electrostatic Force Microscopy

Lynda Patricia Cockins

Master of Science

Department of Physics

McGill University

Montreal,Quebec

2006-08-31

A thesis submitted to the Faculty of Graduate Studies in partial fulfilment of the requirements for the degree of Master of Science.

Your file Votre référence
ISBN: 978-0-494-32681-7
Our file Notre référence
ISBN: 978-0-494-32681-7

ACKNOWLEDGEMENTS

My first two years at McGill have been a very exciting time, both in personal development as well as in learning how to become a good researcher. For their patience, generosity, and kindness, I have a multitude of people to thank.

I would like to thank my supervisor, Dr. Peter Grutter. His generosity has allowed me to pursue my interests unencumbered, and given me the chance to learn about research all over the world. Most importantly, I thank him for giving me the opportunity to work with such wonderful people.

My endless thanks are expressed to Dr. Yoichi Miyahara for being a great mentor, collaborator and friend. Yoichi has been an invaluable resource for our group, providing a seemingly never-ending source of knowledge, dedication, and help to everyone around him. Not only has he helped me in understanding my experiments but he has also been an enormous influence to my development as a scientist.

I would like to thank Dr. Romain Stomp for taking the time to show me how to use the microscope even while in the middle of writing his PhD thesis, and for leaving me plenty of resources in order to get my own research started.

I thank Mehdi El Ouali for donating some of his gold samples to me and to Philip Poole at the National Research Council in Ottawa for his self-assembled InAs

quantum dot sample.

Other McGill members who were involved in this work and who are thanked presently are: Robert Gagnon for the SEM and sputtering machine, John Smeros for always having liquid nitrogen and helium for me, Steve and Eddie from the machine shop who helped make some parts for me and also taught me how to make my own, and to my labmates and the rest of the physics department.

I also was fortunate enough to work with some technicians from Ecole Polytechnique at the University de Montreal, who taught me how to use the focused ion beam. I would like to thank Dominic Cappe, Marie-Helene Bernier, and Jean-Philippe Masse for training me.

NSERC has been very good to fund me throughout various summer terms, this degree, and my future PhD degree and deserves my thanks.

I thank Patricia Davidson for her helpful editorial comments and french translation of my thesis abstract.

Finally, I would like to thank my huge support group of family and friends! In particular, I must thank those who are constantly and endlessly encouraging me: my parents, and my boyfriend Chris Godbout (who is also responsible for the marvelous computer rendered cantilevers in Chapter 4).

ABSTRACT

This work focuses on the atomic force microscope: its hardware, modes of operation, and applications.

The construction of a x-y sample positioner, equipped with position dependent capacitive sensor, is presented. The implementation of a temperature-controlled laser for cantilever detection, via interferometry, is also discussed.

Two modes of atomic force microscopy are used. Amplitude modulation mode images are done in vacuum using Q-control to reduce the apparent Q-factor of the cantilever. Frequency modulation mode is used to obtain non-contact images and force curves above a quantum dot or gold sample. The former leads to detection of single electron charging events from a buried 2D electron gas to the surface layer of the sample. The latter was done to determine the geometric behaviour and capacitance of high-aspect ratio cantilever tips; a method for which is presented where the height, cone angle, radius of curvature and angle to the sample can be controlled.

ABRÉGÉ

Cette thèse a pour objet le microscope à force atomique: son instrumentation, ses modes d'opération et ses applications.

La construction d'un positionneur dans le plan x-y équipé d'un detecteur de position est présentée. La mise en oeuvre d'un laser contrôlable par la température pour la détection par interférométrie de la déflection du cantilevier est également discutée.

Deux modes d'opération du microscope à force atomique sont utilisés. Des images en mode de modulation d'amplitude ont été effectuées sous vide en utilisant un contrôle-Q pour réduire le facteur Q du cantilevier. Le mode de modulation de la fréquence est utilisé pour l'obtention d'images en mode de non-contact et de courbes de force au-dessus d'un point quantique ou d'un échantillon d'or. Dans le premier cas, cela résulte en la détection à la surface de l'échantillon de charge provenant d'un gaz d'électron bi-dimensionnel. Dans le deuxième cas, on obtient le comportement géométrique et la capacitance de pointes hyper pointues. Une méthode pour la fabrication de ses pointes est démontrée, où la hauteur, l'angle du cône, le rayon de courbe et l'angle du cantilevier par rapport à l'échantillon peuvent être contrôlées.

TABLE OF CONTENTS

LIST OF TABLES

LIST OF FIGURES

CHAPTER 1
Introduction

As you start to approach extremely small length scales and enter the realm of quantum physics, there exists an uncertainty in position of small entities such as electrons. Their positions have a finite probability for crossing boundaries such as surface terminations. If a probe is brought close enough to a surface such that the wavefunctions of its electrons overlap with those of the sample, then electrons will tunnel between the two. If a bias voltage is then applied between sample and probe such that it becomes energetically favourable for the electrons to tunnel in one direction, then a tunneling current will be established. Due to the tunneling effect having an exponential dependence on distance, only the probe atom which is closest to the sample will collect current. The probe can be moved over the sample such that variations in current portray surface features, or alternatively the sample can be moved underneath the probe in such a way as to keep tunneling current constant. The above description is of an instrument called a scanning tunneling microscope (STM), which was first demonstrated by G. Binnig, H. Rohrer, Ch. Gerber and E. Weibel in 1982 [1].

A few years later, in 1986, a force sensor was developed by G. Binnig, C.F. Quate and Ch.Gerber and the atomic force microscope (AFM) was created [2]. The probe no longer measured tunneling current as in STM, but the forces arising from the probe-sample interactions. Since forces can be either repulsive or attractive and are additive, the results proved more difficult to interpret as not all of the forces possessed the monotonic decay with distance that exits for the tunneling current.

Although the STM had achieved atomic resolution two years after its invention, AFM would have to wait 5 years before atomic resolution images were achieved (for an illustrated summary see [3]).

Although the most widely used application, AFMs can do a lot more than just imaging! Now researchers are using AFMs to identify the chemical identity of single atoms [4], to look at chemical reactions between molecules [5–8], to move single atoms [9], for single electron detection [10–15], for single electron spin detection [16], for ultra fast images of biological samples [17, 18], and more. Additionally there is a wealth of theories to predict and understand the results that are being obtained. The evolution of the AFM has also led to a number of technological advances particularly to other kinds of sensors, such as cantilever sensors, which operate in the same way as the AFM but now are sensing interactions with molecules in their immersed medium.

The AFM uses a small cantilever (usually a few tens of microns wide and hundreds of microns long) with a small tip on the end (usually with a radius of curvature of a few nanometers) that acts as the force probe. For small deformations the cantilever beam is spring-like, obeying Hooke's Law: $F = -k\Delta x$, where a force, F, causes a deflection, Δx, proportional to the spring constant, k, of the cantilever. Detection schemes, such as laser reflection, interferometry or resistive measurements, allow for the measurement of cantilever deflection or a change in the resonance frequency of an oscillating cantilever. This detectable change is converted into a tip-sample interaction force. For example, a typical spring constant, $k = 1$ N/m, and force of 1 nN will cause cantilever deflections on the nanometer scale which can be detected by a laser system (note that the deflections are small compared to the size

of the cantilever). Later chapters will discuss the measurement of forces using an oscillating cantilever, where forces on the order of piconewtons are routinely measured.

The properties of the cantilever and cantilever tip cannot be ignored in any AFM experiment. In addition to deciding on the geometry and material from which it is made, the cantilever may also require a coating. Coatings usually serve to functionalize the tip, for example in the measurement of magnetic forces the cantilever requires a magnetic tip in order to interact with the sample. More importantly, the geometry of the cantilever tip greatly affects the experimental results and thus must be optimized. As a prime example, consider the main technique used in this thesis where a branch of AFM, called electrostatic force microscopy, is used to measure the long ranged electrostatic forces of a sample. Here, the cantilever typically has a conductive layer in order for a bias voltage to be applied between tip and sample as the electrostatic force is voltage dependent. In addition, a conductive tip will form a capacitor with a conductive sample which will have contributions from not only the tip apex, but the tip's sides as well (which are of little interest when trying to detect very small effects). In addition, many researchers with an interest in images will demand that the tip radius be as small as possible as this influences the minimum sized features that can be resolved. High aspect ratio tips can not only have a small radius of curvature but are also long and thin to image deep sample features or to reduce the contributions of long ranged forces. To this end, some groups have attempted affixing or growing carbon nanotubes to the ends of cantilevers [19–22].

Carbon nanotubes can have radii on the order of a few nanometers and can be conductive, however some types are semiconductors and others even insulators,

making a number of the carbon nanotube tips unusable as conductive tips. In addition, electrostatic force microscopy requires electrical contact to the tip. In the case of carbon nanotube tips this process is not always robust and can again yield some defective tips.

Another approach to making high aspect ratio conductive cantilever tips is to use a focused ion beam (FIB) to shape the tip of the cantilever (see the appendix for how a FIB works). Such a technique was first introduced in 1987 by Biegelsen et al. in order to remove oxide from tungsten STM tips (tungsten wires) [23]. It was found that the FIB tips had smaller radial curvature, little or no oxide on the tip surface, and were more reproducible than electrochemically etched tips: the standard fabrication process at the time. They later refined their technique to produce a tip which was almost atomically sharp [24]. In 1991 Vasile et al. used a FIB to create a high aspect ratio STM tungsten tip whose purpose was to image deep sample trenches [25]. Demanding reproducibility, they created high aspect ratio tips of height 6 μm, with radii of curvature between 4 and 30 nm and cone angles between 8° and 20°. They also tried the technique with PtIr wires and observed less irregularities compared with the tungsten tips and suspected this was due to grain size. In 2005, Akiyama et al. would glue a tungsten wire onto an AFM cantilever and then use the technique reported by Vasile et al. to create a high aspect ratio metallic cantilever tip for use in non-contact AFM [26]. With patience, they obtain radii of curvature of less than 5 nm. As they used the tip in an ultra high vacuum, it needed to survive heating up to 900°C, after which it produced atomically defined images. They noted

that the heating step could be skipped if a PtIr tip was used as it is less vulnerable to oxidation.

A competing approach to a high aspect ratio tip was developed by Menozzi et al. where the FIB mills a small hole completely through the cantilever, starting at the tip, and a metal is deposited into this hole and electrically connected along the backside of the cantilever [27]. The tip side of the deposited metal is shaped into a sharp tip. Using this method they accomplished a reduction in the force contribution from the sides of the cantilever as well as from the cantilever itself by having only a small area of the cantilever being coated with a conductive strip. Pingue et al. further developed this technique by placing a metal coating on the tip-side of the cantilever (but avoiding the tip) that would be electrically connected to the sample, thereby electrically shielding the cantilever from contributing to the force measurement [28]. In this thesis, the approach taken by Pingue et al. is not pursued as the contribution to the force from an oscillating cantilever is small when the tip is close to the sample, and thus is a lot of effort for a very small, if not undetectable, change in the measured force. In addition, the conductivity of the FIB deposited metal is not well known for temperatures as low as 4 K, in which environment our experiments are typically executed.

This thesis explores the use of a high aspect ratio tip for the measurement of electrostatic forces in an effort to reduce the parasitic background arising from the contribution to the force from the sides of the cantilever tip. The motivation for such a pursuit is to improve the detection of single electron events [15]. The technique combines the work of Vasile et al. [25] and Akiyama et al. [26] in order to glue a

wire onto a cantilever which is shaped by the FIB, with one important difference. In order to further reduce stray force contributions, the angle between the cantilever tip and the normal of the sample, typically about 15°, is eliminated. A PtIr wire is used as it is not easily oxidized. This technique was chosen as the PtIr wire should be conductive at temperatures as low as 4 K, but the conductivity of the other kinds of tips (carbon nanotube or FIB deposited metal) will not necessarily be so.

This thesis explores multiple aspects of AFM and is presented in chronological order. This work began with the building of new AFM components for our home built AFM, and was followed by a rigorous sequence of updates for the preexisting model. At the same time a novel technique for fabricating high-aspect ratio cantilever tips with controllable angle was developed. These tips would be used for the detection of electrostatic forces which, due to their long ranged nature, would interact, sometimes significantly, with the sides of the cantilever tip. These stray interactions would muffle small features of interest and so are undesirable. Making a high-aspect ratio tip serves to improve the quality of one's measurements because this background interaction is reduced. Before testing the tips, experience in how the AFM works was acquired through learning different ways in which to take images by operating the AFM in two different modes: frequency and amplitude modulation modes. The fabricated tips were then tested and compared with theory, revealing that these tips did behave as high aspect ratio tips. In the last section of this thesis an outlook of future experiments is alluded to and some recent results of spectroscopy over semiconductor quantum dots (nanometer sized regions of localized charge) are shown where single electron events are detected.

CHAPTER 2
Atomic Force Microscopy

2.1 Forces We Measure

There are a number of forces that can be measured with an AFM: van der Waals forces, electrostatic forces, magnetic forces, capillary forces, frictional forces, etc. In this thesis, only van der Waals, electrostatic and repulsive forces were studied and will be described.

2.1.1 Van Der Waals Forces

Van der Waals (vdW) forces arise due to dipole-dipole interactions between atoms when they become instantaneously polarized. If the cantilever tip is modeled as a sphere, of radius R, approaching a planar sample a distance z away, then the magnitude of the force for small separations (i.e. $z \ll R$) would be [29]:

$$F_{vdW} \sim -\frac{HR}{6z^2} \tag{2.1}$$

Where H is the Hamaker's constant, which is on the order of 10^{-19} J for interactions across vacuum, and depends on the dielectric constants of sample, tip and surrounding medium. The sign of H can also be different depending on the values of the dielectric constants, making the usually attractive vdW forces repulsive (see [30] for an experimental realization). For large separations, the retardation of the vdW force causes the tip-sample force to decay faster, by a factor of $1/z$ [31]. For comparison, the force on a conical tip has a $1/z$ dependence at small separations and thus a $1/z^2$ for large separations [31]. For an estimate of the order of magnitude of the

vdW force, consider a spherical tip of radius $R = 30$ nm, with $z = 20$ nm, then $F_{VDW} \sim -1$ pN. Due to its small magnitude, vdW forces can only be detected in our experiments when the tip is very close to the sample. One note to make is the Hamaker's constant is not constant with separation size and after ~10 nm is already about 1/2 of its nonretarded value [29].

2.1.2 Electrostatic Forces

Mainly we are interested in the electrostatic force. The electrostatic force is a long-ranged force (measurable hundreds of nanometers away from the sample), that arises due to the energy stored in separating charges. Since the electrostatic force is voltage dependent, conductors are usually present in order to controllably probe the force. Both tip and sample usually have a conductive layer and are held apart forming a capacitor C. The conductors (e.g. tip and sample) are held at constant potentials by external batteries. Changes in the system, for instance an increase in the tip-sample gap z, cause the batteries to do work to maintain the constant potential ΔV between the capacitor. The free energy of such a system is $U = -\frac{1}{2}C\Delta V^2$. Since the electrostatic force is the negative gradient of this energy, the force along the axis connecting tip and sample is then:

$$\mathrm{F_{es}(\Delta V, z)} = \frac{1}{2}\frac{\partial \mathrm{C}}{\partial \mathrm{z}}\Delta \mathrm{V}^2 \tag{2.2}$$

An extended study of this force, which includes the effects of some point charges between tip and sample is discussed by Kantorovich et al. [32]. Since the tip and sample are quite often not the same material and furthermore can be subject to

trapped charges, debris, surface effects, etc, there is a difference in the work functions between the two that offsets the minimum of the force parabola from $\Delta V = V_{tip} - V_{sample}$ to $\Delta V = V_{tip} - V_{sample} - V_{CPD}$. V_{CPD} is the contact potential difference, which for our experiments has been measured between 200 - 500 mV for a variety of tips and samples.

To get an idea of the limiting behaviour of the electrostatic force consider Hudlet et al.'s [33] results for a conical tip with spherical apex. They derived a formula for the total electrostatic force felt by such a tip that included the height, H, half cone angle θ and radius R of the tip (Figure 3–1(a)). They found that for $z \ll R$ (small tip-sample gap) the tip-sample force varied as $\pi\epsilon_o R/z$, and for $z \gg R$ (large gap) the force varied as $\pi\epsilon_o k^2 \ln(H/z)$ where $k = (\ln\tan(\theta/2))^{-2}$. This showed that at close distances the force was dominated by interactions between the sample and the tip apex, but as the tip-sample distance reached R and beyond the interaction force is described more by the geometry of the tip, here from the conical shape. Comparison to the vdW force (above) gives the same geometrical dependence for a conical tip when the gap between tip and sample is small, but at large separations the electrostatic force interacts more strongly with the tip as seen in our experimental results (e.g. section 4.2).

The total measured force from both contributions:

$$\mathrm{F} = \mathrm{F_{es}} + \mathrm{F_{other}} \tag{2.3}$$

where F_{other} are forces other than the electrostatic force (e.g. the vdW force). Experimental curves for $F(\Delta V, z)$ are shown in section 4.2.

2.1.3 Repulsive forces

A brief explaination will be given as repulsive forces are measured during some types of amplitude modulation mode images which will be described later. Repulsive forces arise when the tip is close enough to the sample surface such that the electron wavefunctions can overlap and, due to quantum mechanical effects, are strongly and increasingly repelled from each other. A formula describing the exact distance dependence is lacking, however empirical equations model the potential as either a power law or exponential function. For example, the three most common potentials are [29]:

1. Hard Sphere Potential: $U(z) = (\sigma/z)^n, n = \infty$
2. $U(z) = (\sigma/z)^n, n\epsilon I$
3. $U(z) = ce^{-z/\sigma_o}$ where c and σ_o are adjustable constants.

Another common way in which to treat the entire potential (including both attractive and repulsive terms) is with the Lennard-Jones potential: $U(z) = 4\epsilon[(\sigma/z)^{12} - (\sigma/z)^6]$, where σ is the hard sphere diameter.

2.2 Cantilevers for Atomic Force Microscopy

Crucial to the understanding of how forces are measured in dynamic force microscopy is in the understanding of the behaviour of the cantilever. For small displacements, z, the cantilever is a linear spring following the equation of motion:

$$\mathrm{m\ddot{z} + \gamma\dot{z} + kz = F_{applied} + F_{ts}(z(t)) + F_{th} + F_{noise}} \tag{2.4}$$

where $F_{applied}$ is the force applied to the cantilever (the driving force), F_{ts} is the force on the cantilever from the sample, m the effective mass of the cantilever, k the spring constant, and γ the dissipation coefficient. F_{th} and F_{noise} are the forces due to thermal motion and external vibrations respectively and will be neglected in further analysis. A periodic applied force, $F_{applied} = F_o \cos(\omega t - \phi)$, results in a resonance curve for the cantilever which is characterized by a resonance frequency $\omega_0 = \sqrt{k/m}$, and quality factor, $Q = m\omega_0/\gamma$. Alternatively Q is the full width at $1/\sqrt{2}$ of the maximum amplitude of the lorentian resonance curve and so describes the sharpness of the peak, i.e. $Q = \omega_0/\Delta\omega$. The resonance curve of the cantilever, due to the periodic applied force, oscillates with the amplitude [34]:

$$\mathrm{A}(\omega) = \frac{\mathrm{F_o/m}}{\sqrt{\left(\omega_\mathrm{o}^2 - \omega^2\right)^2 + \left(\omega\omega_\mathrm{o}/\mathrm{Q}\right)^2}} \tag{2.5}$$

A graph of the resonance curve of the cantilever is shown below in Figure 2–1. Note that the resonance occurs at a phase of $\pi/2$.

Depending on the forces of interest and the sample of study, the preparation and experimental setup are quite different including the required type of cantilever and cantilever tip. For example, some modes require a cantilever with a low Q-factor ($\leq$500), whereas others benefit from a cantilever with a much higher Q-factor for reasons that will be explained in section 2.3.1 and section 2.3.2. Contact AFM, where tip and sample are in contact, requires a robust cantilever tip so that it can withstand approach and contact with the sample, whereas in non-contact AFM this requirement is not as vital. In general a sharp-tipped cantilever is desirable because the thickness of the tip determines the size of features that one can resolve.

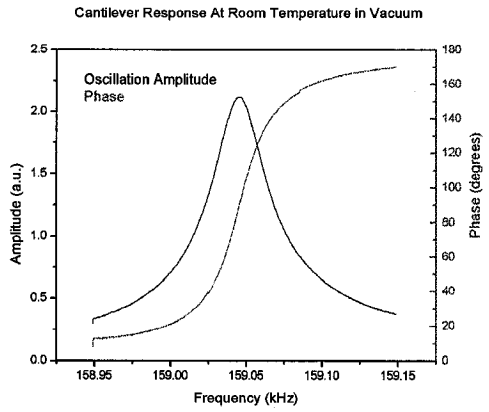

Figure 2–1: Cantilever response to a periodic driving force. This is experimental data. Here, the cantilever had a Q of 3180 and a resonance frequency of 159,046Hz. The data was taken at room temperature in vacuum. An arbitrary constant was subtracted from the phase value to emphasize that the amplitude is maximized at a phase of 90°

However this is not always the case as for biological samples sometimes one wants to make contact to the specimen without puncturing the sample and so a rounded tip (typically a glass bead) is glued onto the cantilever. Even the material of the cantilever needs to be chosen with some care. Typically, silicon cantilevers are batch fabricated and sold commercially with a variety of properties, including functional coatings. The cantilever could be coated for a variety of purposes: to make molecules bind to them (to pull apart molecules, for example), to deposit material onto the surface, to increase the strength of the cantilever (e.g. diamond coating), or to make the cantilever electrically conducting as is done in electrostatic force microscopy.

2.3 Dynamic Force Microscopy

There are two main operating modes of AFMs: Static and Dynamic. Static AFM refers to detecting a static deflection of the cantilever, where the force is proportional to the deflection since the cantilever obeys Hooke's law, $\Delta x = -F/k$, where k is the spring constant of the cantilever. The advantage of this mode is in the ease of image interpretation since the force and deflection are proportional. However, long-ranged attractive forces make it difficult to avoid jump-to-contact with the sample, most often in the area of highest interest, and special techniques have to be used to obtain good images [3, 30].

Only dynamic modes have been used during this thesis. The distinguishing characteristic of dynamic force microscopy (DFM) is that the cantilever is oscillating. There are two main types of such operation: amplitude modulation and frequency modulation. In DFM, force gradients are sensed by monitoring the oscillation of the cantilever in close proximity to the sample. These gradients cause a change in the spring constant of the cantilever, which in turn alters its resonance frequency [34].

2.3.1 Amplitude Modulation Atomic Force Microscopy

Amplitude modulation (AM) involves driving the cantilever with a fixed signal of constant amplitude, frequency, and phase close to the resonance frequency of the cantilever [35]. Interactions with the sample cause the resonance frequency of the cantilever to shift, decreasing the amplitude of oscillation and changing the phase with respect to the driving signal. It takes some time for the cantilever to obtain a new steady state oscillation since it must dissipate energy in order to reduce its

amplitude of oscillation. This amount of time is described by the time constant $\tau = 2Q/\omega_o$. Since the Q of the cantilever is inversely proportional to the dissipation it shows up in the time constant. Making the Q dependence explicit serves to highlight the disadvantage of this technique: although increasing the Q of the system increases the signal to noise ratio, it also limits the maximum imaging speed [36]. For example, consider a cantilever with a resonance frequency of roughly 150kHz, and a Q of 500 in air and $100,000$ in a vacuum at 4K (Q increase with different environmental conditions is explained in section 3.2). The value for τ will be roughly 0.01sec and 1 sec respectively meaning that the cantilever requires that much time to respond to features. Experimentally, this means that an image is going to take a sufficient amount of time so that one has to worry about drift (e.g. of the sample, cantilever resonance frequency, e.t.c.) as a typical image of 256x256 pixels could take several hours if each pixel requires 1 second for allowing the cantilever to respond.

We sometimes do a type of AM mode, where the cantilever is close enough to the surface to briefly come into contact with the sample over one period of oscillation, called intermittent contact or tapping mode (Tapping mode is a registered trademark of Digital Instruments Inc.). To be complete, it should be mentioned that tapping mode does not necessarily require contact with the sample; as long as the cantilever enters the repulsive force regime while imaging it is still considered to be in tapping mode. With the cantilevers we use, images can be done at room temperature in air, or at liquid nitrogen temperature in He gas, but not at liquid helium temperature because the Q would be too high. In fact, we use the same type of cantilevers for all of our experiments which require either a high or low Q factor. We use higher Q

cantilevers and reduce the Q by operating in Q-Controlled mode to do the imaging in vacuum conditions. This technique allows us to do images at 77 K in vacuum and at 4.5K in He gas. See table 3-1 for typical Q values in various environments and section 3.3.2 on Q-Controlled AFM.

2.3.2 Frequency Modulation Atomic Force Microscopy

Frequency modulation (FM) mode was invented by Albrechet et al. in 1991 [36] to overcome the problem of the speed limitations of AM mode. In this mode, a feedback loop measuring the response of the cantilever maintains its oscillation at its resonance frequency. The feedback loop takes the amplified and phase-shifted frequency response of the cantilever and reapplies this signal to the cantilever. The cantilever will respond mainly to the resonance frequency, causing this frequency component to be amplified more than the others. This frequency is then given a phase shift of $\pi/2$ (optimized manually by reducing the amount of energy required to maintain oscillation, i.e. the dissipation), which is required for the cantilever to be on resonance. Of course, there are neighboring frequencies amplified as well, the extent of which is determined by the cantilevers Q factor, such that a higher Q is more like a delta function and has a more narrow range of amplified frequencies. The changes in resonance frequency, due to interactions with the sample, are detected by a phase locked loop (PLL) which acts, in our case, as a frequency detector. Figure 2–2 shows the block diagram of the feedback used to maintain the oscillation of the cantilever. The PLL output is converted to a voltage for the piezotube. Alternatively, one could also use the PLL output to drive the cantilever at its resonance frequency. The time

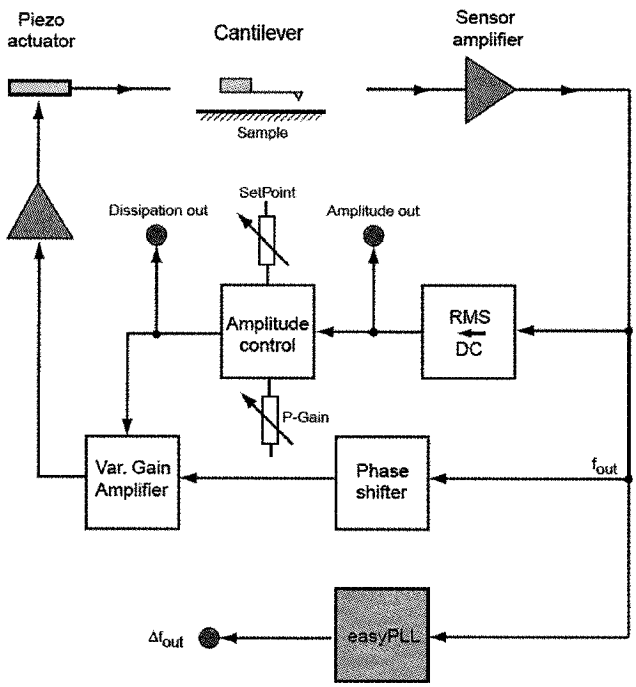

Figure 2–2: A simplified block diagram of 'self-oscillating mode', so called as the detector (in our case an interferometer) signal is used to maintain oscillation. The setpoint, P-gain and phase shifter are manually chosen. The phase is set to minimize the dissipation, thereby ensuring the cantilever is on resonance. The variable gain amplifier sets the amplitude of the cantilever oscillation which is achieved by the phase shifted detection signal being multiplied with the dissipation signal. The PLL provides the frequency shift which can then be converted into the proper voltage to send to the piezotube scanner. This block diagram was taken from the PLL manual. [37]

constant required by the cantilever to obtain its new steady state oscillation is only $\tau = 1/f_o$, which is much less than in AM mode [3,36]. A Q independent bandwidth allows measurements to be done in vacuum, where the Q of the cantilever can get very high since its motion is not being damped by a medium. A high Q is desirable since increasing the Q decreases the noise as shown by Albrecht et al. [36] who gave an equation for the cantilever's thermal noise in the frequency shift as being inversely proportional to the square root of Q.

2.4 Design and Improvements to the Home-Built AFM

2.4.1 Design

Our home-built AFM was designed for use in temperatures as low as 4 K by placing the microscope, which is sealed inside a vacuum can, in a liquid helium bath. It also works at liquid nitrogen and room temperature at, or below, atmospheric pressure and under applied magnetic fields up to 8T (only at liquid helium temperature as it is a superconducting magnet). Complete details of the design can be found in Dr. M. Roseman's Masters' [38] and PhD thesis [39], published here [40], and additional improvements were made as commented on in Dr. R. Stomp's PhD thesis [41].

The main components of the microscope hang from a vibration isolation bellows. This serves to reduce noise from mechanical vibrations. Detection of the cantilever oscillation is done via an interferometer, similar to the fiber interferometer reported in [42] and [43], which requires approach of a fiber optic towards the tipless side of the

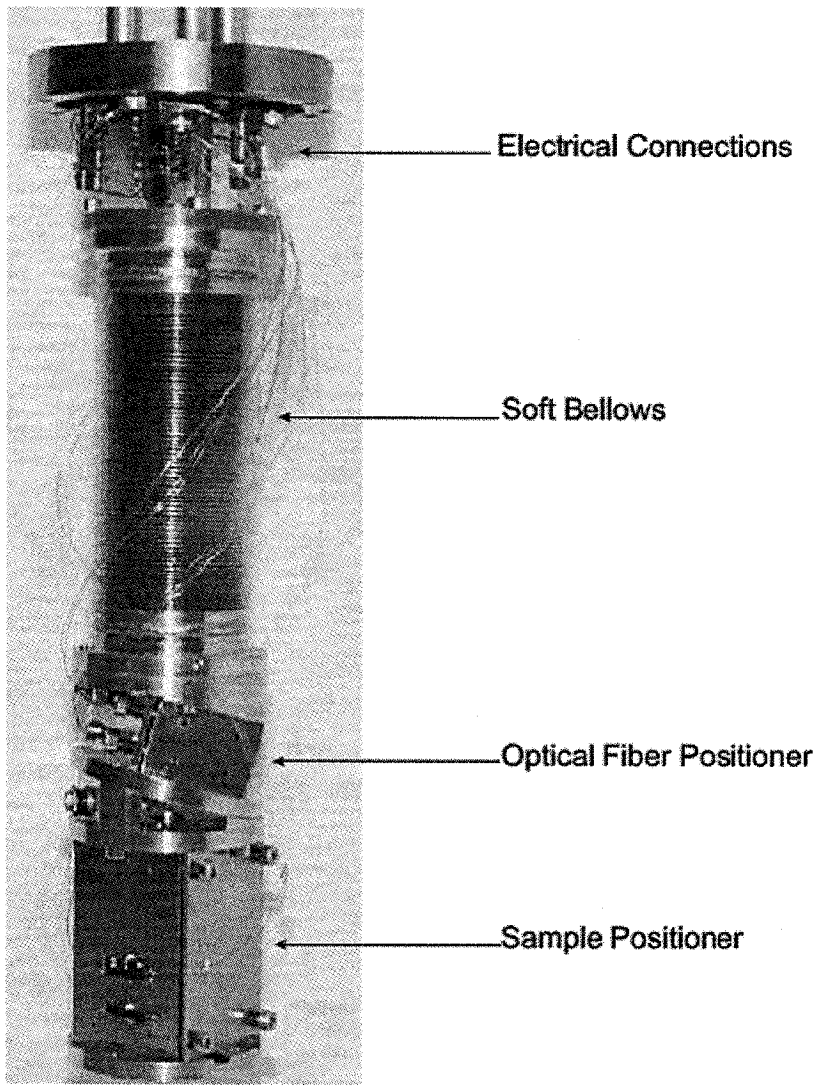

Figure 2–3: Picture of the microscope showing the bulk of the microscope hanging from the bellows. Photo taken from [39]

cantilever. The optical fiber coarse approach mechanism, called a 'fiber walker', is based on a piezoelectrically driven stick-slip walker. Similarly, the sample is coarsely approached towards the cantilever by four pairs of shear piezo stacks, called a 'sample walker', and then finely approached with a piezotube positioned underneath the sample which is also responsible for moving the sample underneath the tip in a raster scan fashion.

The cantilever is glued, using silver paint, to a bimorph actuator on an angle of 15° from the normal of the sample. The position of the cantilever is fixed and is approached by the optical fiber and sample. A picture of the microscope is shown in Figure 2–3 where the bellows is plainly visible. The rectangular structure at the bottom houses the sample and sample positioning system. The smaller, tilted, rectangular box that is directly connected to the bellows, houses the fiber optic and its positioning system. Inbetween these two positioners, where a gap in the figure can be seen, is where the cantilever resides.

2.4.2 Improvements

Currently, this microscope is undergoing some drastic changes and replacements. The microscope reacts to applied magnetic fields which could be due to slight magnetization of the 'non-magnetic' stainless steel frame (grade 304L) and other components of the microscope which can be magnetized (e.g. the screws in the microscope). As future experiments will utilize the superconducting magnet at the bottom of the dewar, the microscope has to be rebuilt out of titanium. This provided us with the opportunity to make some improvements. Andre Brown began the design of a

new scanning piezotube mount for the sample which would allow not only coarse approach in z, but also $x - y$ positioning capabilities, shown in Figure 2–4. A key limitation to the design was the restricted space inside the dewar. Unsatisfied with the cumbersome way in which the four shear piezo stacks responsible for horizontal motion would be repaired, we designed a removable titanium plate to be inserted into the base of the frame as shown in Figure 2–5(b), upon which three newly designed shear mode piezo stacks (Figure 2–5(a)) could be glued to allow motion of the sample in the x-y plane. Repairs to the piezo stacks can now be done more easily and effectively with the removable plate as they are easily accessed, and should the stacks need to be replaced entirely the old stacks are now more easily removed. This is important because thermal cycling of the microscope sometimes leads to glued components popping off (piezoelectric materials or wires from the electrode) due to thermal expansion coefficient mismatches.

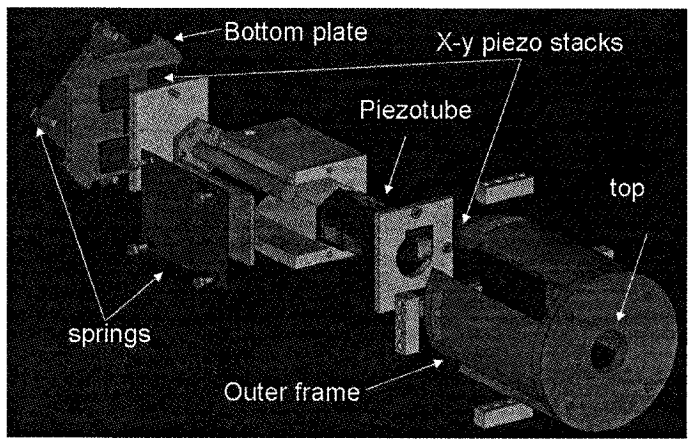

Figure 2–4: Orginal AFM Sample Walker Design by Andre Brown

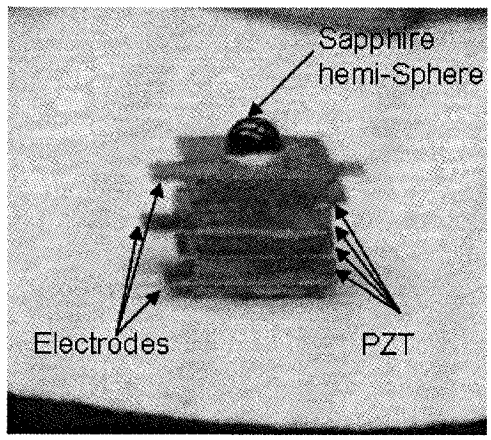

(a)

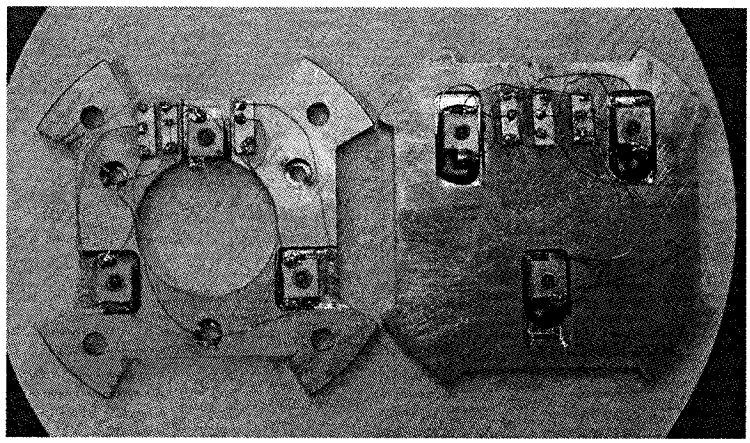

(b)

Figure 2–5: Shown in (a) is a close up of a piezo stack. (b) shows the new top plate and removable bottom plate (compare to Figure 2–4) with the piezo stacks glued on and wired up.

The implemented new design of shear-piezo stacks, Figure 2–5(a), are now routinely used in the lab for various systems because they offer some key advantages over the previous design. The new design uses metallic foil electrodes between piezo layers to make electrical contact as opposed to connecting directly to the piezo. It is not only much simpler to glue to the electrode, but the possibility of causing a short circuit is much less reduced by this design. Specifically, there are 4 layers of lead zirconate titanate ceramic (PZT) (thickness 0.73mm), 5 layers of CuBe electrodes (thickness 0.11mm) sandwiching the PZT, and there is an alumina base (thickness 0.5mm) to prevent electrical contact with the microscope. The PZT we chose had a curie temperature of 300°C to withstand heating to 140°C in order to cure the silver epoxy (EPO-TEK H20E) between the layers. To ensure that there is no conductive glue bridging the layers, these stacks are easily filed to remove extra glue. Small sapphire hemispheres were glued to the top of the stacks ensuring that each stack would contribute equally to the x-y movement of the sample walker.

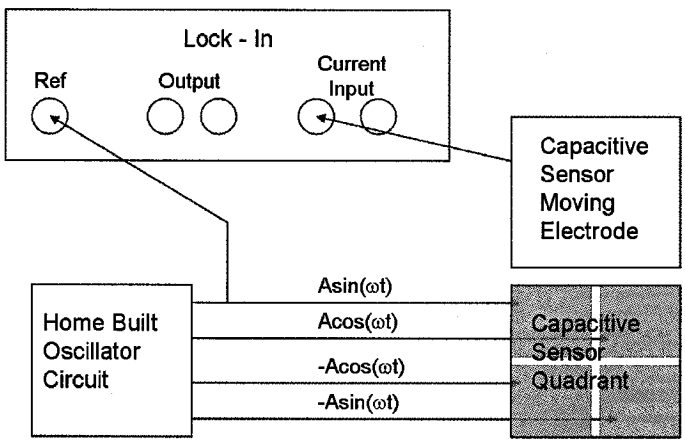

Figure 2–6: Experimental set-up for determining the movement of the sample walker using a capacitive sensor. This setup was used to collect the data in Figure 2–7(a)

A capacitive sensor was implemented to detect the position of the sample once inside the dewar. The x-y capacitive sensor [44] consists of two copper plates separated by less than a few millimeters, one divided into four quadrants. By sending phase-shifted voltage signals (each of the four signals is shifted by $\pi/2$) to each of the 4 quadrants the resulting current detected by the moving electrode is proportional to the area of overlap with each quadrant. A Burr-Brown 4423 precision quadrature oscillator was used to create a circuit with 4 sinusoidal outputs at 0°, 90°, 180°, and 270°, and a lock-in amplifier (Stanford Research Systems Model SR850 DSP) was used to detect the current in the moving electrode (the BB4423 circuit is explained in [44]). The in-phase portion of the current results from movement along one axis while the out of phase component results from movement along the other. In order for the motion to be proportional to the current, the phases have to be -45°, 45°, 135°, 225° which is accomplished one of two ways: either by gluing the moving electrode diagonally to the quadrant, or by using a sine wave shifted by 45° as the lock-in's reference signal. The experimental setup is shown in Figure 2–6. The lock-in was operated with a time constant of 1 second, and 100 nA sensitivity. The voltage signals sent to the capacitive sensor were all of 10 V amplitude and 10 kHz frequency. The sample walker was completed and the capacitive sensor was tested at room temperature in air. Calibration of the step size at various temperatures will be done once the sample walker is used as the main sample positioner in the AFM. The graph in Figure 2–7(a) shows the preliminary test where the sample was first moved in the forward, and then backward, y direction. The axis opposite the motion showed that the sensor's position stayed fairly constant, where slight movement along this

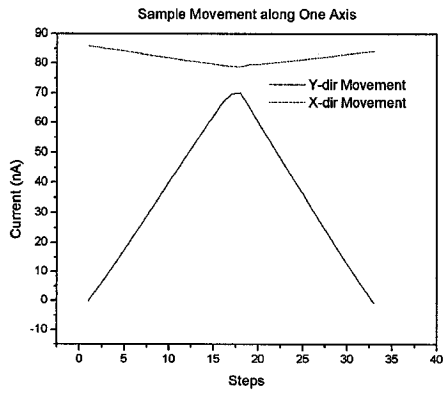

(a)

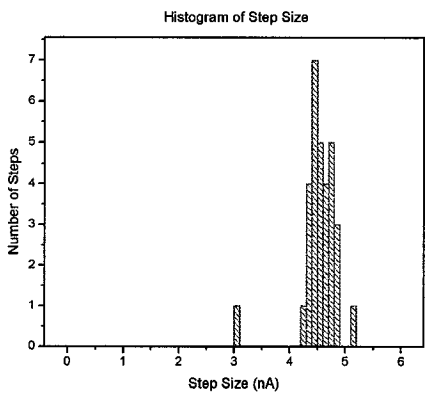

(b)

Figure 2–7: Capacitive X-Y Sensor Data Mounted on the sample walker. Data taken in air at room temperature. (a) shows the movement of the sample holder along one axis. Note the slight movement in the opposite axis. (b) is a histogram of the step size measured in nA. Note the sharp distribution with a mean value of 4.5nA and standard deviation of 0.3.

axis is due to misalignment of the moving electrode to the quadrant electrode. This can be corrected by optimizing the phase of the reference signal. From this test the actual step size was not easily determined, however Figure 2–7(b) shows a histogram of the steps with a fairly constant step size in nA. This sample holder will not only allow us access to new areas of the sample (which prevents unnecessary handling of the sample), but it may even allow us to include more than one sample of study to be mounted for low temperature experiments.

A new laser was installed for the detection of the cantilever motion. The wavelength of the laser was increased from 780nm to 1550nm. This new laser provided an increase in the sensitivity of the detector, where the formula for the sensitivity S is given by Eq. (2.6) in V/nm below [45].

$$S(V/nm) = \frac{2\pi V_{pp}}{\lambda_{laser}} \tag{2.6}$$

Where V_{pp} is the peak to peak voltage of the interferometry signal and λ_{laser} is the wavelength of the laser. The obtainable peak to peak voltage of the interferometry signal increased from 2 - 3V (old laser) to 10 - 13V, giving an improvement by a factor of 2.3. The new laser is temperature controlled, meaning that the laser wavelength will be less prone to drift which increases the dissipation of the system. As future experiments will study the dissipation in greater detail, this new addition is very useful. Control of the temperature allows us to fine adjust the wavelength of the laser to maximize sensitivity [45]. The new laser is also radio frequency (RF) modulated in order to reduce its coherence. Applying a voltage that is RF modulated changes the wavelength of the laser rapidly so that it is no longer narrowly defined,

making it less coherent. If very coherent laser light is back reflected through the fiber, it will stimulate emission of more light which can change the lasing wavelength in several ways, one of which is by changing the cavity length (as it is heated due to the higher power inside), which in turn increases the laser noise. A key advantage of a 1550 nm wavelength is that there are many more, and less expensive, components that can be purchased for this laser since it is within the telecom range.

2.5 Noise of the Detection System

The power spectral density of the new laser displayed in both $nV_{pp}/\sqrt{Hz}$ and $fm/\sqrt{Hz}$. The spectra were taken with a Stanford Research Systems Model SR770 FFT Network Analyzer at room temperature in a vacuum with a non-excited cantilever whose resonance frequency was approximately 150 kHz. When the laser is turned on, a laser intensity noise contribution is apparent in the first 10 kHz (the approximate value of the corner frequency) and follows a power law relationship where the exponent is $\sim$-0.6. This low frequency noise component is so large that it saturates the analyzer and thus does not display the level of noise properly, because of this it is not shown here. This can be corrected by first filtering out the low frequency noise by using a high-pass filter, which is shown in figures 2–8(a) and 2–8(b). The resolution of the laser system is approximately 50 $fm/\sqrt{Hz}$.

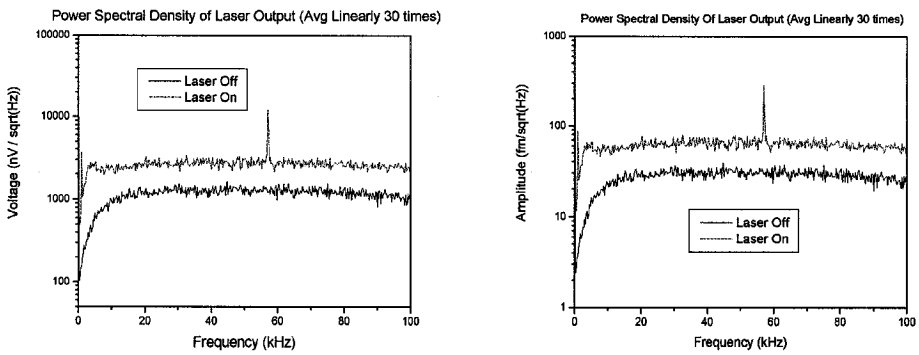

(a) (b)

Figure 2–8: Power spectral density of laser noise at room temperature in vacuum. The spectra is taken for a non-excited cantilever with resonance frequency around 150kHz. The analyzer can only display the noise up to frequencies of 100 kHz. The laser signal has been high-pass filtered and so the lowest frequency components are reduced, causing the plot to curve downwards at low frequencies. A noise source is apparent at approximately 57 kHz which is most likely due to mechanical vibrations.

CHAPTER 3
Experimental Procedure

Electrostatic force microscopy (EFM) provides information about the electrostatic forces of the sample, giving additional information than the topography alone. For example, EFM provides spatially localized detection of charges with single electron sensitivity [10, 11], detection of scattering centers in mesoscopic devices [46, 47] as well as charge traps on semiconductor surfaces [12–15]. The high aspect ratio tips have been tailored for use with this technique for the eventual analysis of semiconductor self-assembled quantum dots (see Chapter 4). Although the main purpose of this section is to describe the preparation and realization of EFM experiments, a small section on Tapping mode (section 3.3.2) is included in order to compare images from the two techniques.

3.1 Cantilever Considerations

As stated earlier, EFM requires metallically coated cantilevers and tips as the force is voltage dependant. We coat our cantilevers with 10 nm of titanium and 10 nm platinum. We chose platinum because it is not easily oxidized (unlike tungsten) which serves to blunt the tip apex. The titanium layer serves as an adhesive layer for the platinum. We then check our cantilevers in a scanning electron microscope to make sure that there is no large debris on the tip of the cantilever. Although we are principally measuring the interaction with the apex of the tip, electrostatic forces are long ranged forces and other parts of the tip, for example the sides of the tip, can contribute to our measurement making the results more difficult to interpret.

Typically, these side walls are characterized by a 'half-cone angle' as depicted in Figure 3–1(a). Hudlet et al. published two formulas: one for the force on the apex of a conical tip, and one for the force contribution of the sides of the tip [33]. A ratio of the tip-apex force to the total force as a function of tip-sample gap for various half-cone angles demonstrates that a reduction in cone angle relatively increases the force felt by the tip apex (Figure 3–1(b)). These results set the foundation for this thesis by alluding to the fabrication of a high aspect ratio tip to be explained in detail in section 4.

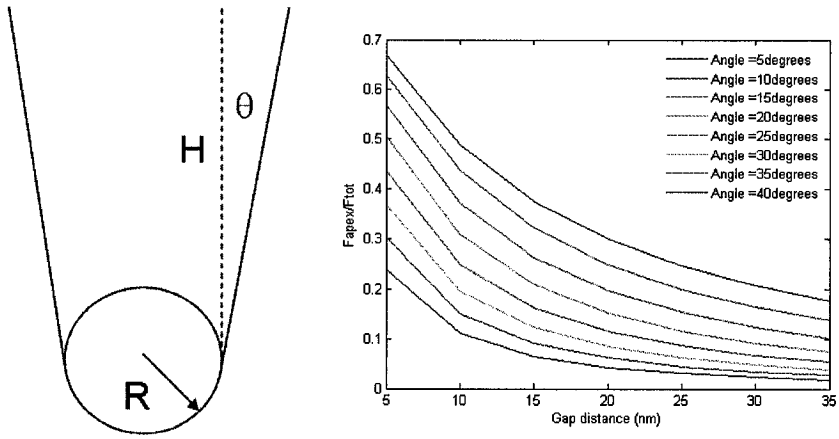

(a) (b)

Figure 3–1: The dimensions of the modeled cantilever tip (a). (b) is the ratio of the force on the tip apex to the total force versus tip-sample gap (nm) plotted for various half-cone angles (displayed in the legend).

3.2 Experimental Procedure

Once the proper cantilever is selected, its tipless side must be aligned with the cleaved end of an optical fiber. Cleaving the fiber causes approximately 4% of the

laser light to be back-reflected through the fiber at the glass-air interface. We do not know experimentally the power of the back-reflected light as we do not have a power meter for 1550 nm wavelengths in our lab. Once the cantilever is aligned with the fiber, a certain amount of laser light will reflect off of the backside of the cantilever and reenter the fiber. This reflected light then interferes with the back-reflected light and the interference pattern is measured by a photodiode. The current emitted by the photodiode is this signal and is converted to a voltage that we measure. To have the most sensitivity, the fiber is positioned such that it is located at the steepest part of the sinusoidal interference curve (e.g. $\sin(\pi/4)$). The value of the peak-to-peak interferometer signal gives the sensitivity of the fiber-cantilever setup (see Eq. (2.6)). Typically, we can get a peak to peak voltage of 10 V (although there has been instances as high as 14V) and with the wavelength of the laser being 1550 nm, the sensitivity is 0.04 V/nm. The noise of the laser when light is being reflected off of a non-excited cantilever is usually between 1 - 2 mVrms. The sensitivity is good enough to allow us to oscillate the cantilever in the tens of angstroms range and maintain stability.

Now that we have a way to detect the cantilever we oscillate it using a small piezo, called a bimorph, which shrinks or expands along one axis depending on the polarity of the applied voltage. We can sweep the frequency of the applied signal and measure the response of the cantilever to obtain the resonance frequency and Q factor for this specific cantilever. These values change as we reduce the temperature and pressure such that at lower pressures and temperatures both f_o and Q increase (see the chart below). Once these parameters are recorded, we set the cantilever

into 'self-oscillating mode'. In this mode, the cantilever oscillates at its resonance frequency and the amplitude is maintained by a feedback loop. The dissipation of energy by the cantilever is minimized by changing the phase of this signal being sent to the bimorph of the cantilever. The final step, before approaching the sample to the cantilever, is to make sure that the frequency shift being measured by the PLL is as close to 0Hz as possible, reducing the offset in the frequencies measured.

Table 3–1: Cantilever f_o (kHz) and Q for various Temperatures and Pressures

Cantilever f_o (kHz) and Q for various Temperatures and Pressures. The first acronym is the temperature: RT is room temp, LN is liquid nitrogen temp, and LH is liquid helium temp, while the second is the pressure: Atm is atmospheric pressure, and LP is low pressure. Note at LN, the Atm is from He gas (since air would freeze) which does not decrease the Q as much as air if both are at the same pressure since He gas is less viscous.

Cantilever	RT, Atm	RT,LP	LN, Atm	LN, LP	LH, LP
1	-	147.5, 4471	148.3, 9000	145.3, 30000	148.3,50000
2	132.5, 716	132.5,1600	133.3,1100	133.4, 17000	-
3	150, 735	154.3, 4400	-	155, 52000	-
4	-	159, 3180	-	159.9, 32000	159.9, 80000

The entire microscope at this point is mounted inside a vacuum can which is lowered into the cryostat and is no longer visible. A vacuum pump brings the pressure inside down to approximately 10^{-4} mbar and then the sample is heated to roughly 120°C for one hour in attempt to rid it of some of the covering water layer.

To approach the sample, we use an automatic approach system that is built into the Scanita software. The sample is sitting on the xyz scanning piezotube, which in turn is moved up or down by a course approach system consisting of shear-mode piezo stacks. We determine the course-approach step size using a function generator

and Scanita triggers the function generator in order to approach the sample. The piezotube is completely retracted during the course approach step, but following each step Scanita sends a voltage signal to expand the piezotube towards the cantilever. If the cantilever is close, a negative change in frequency is detected and the approach stops. In this way the tip of the cantilever is carefully approached so that we can prevent crashing of the tip. We also tend to set the sample bias voltage fairly high (3 V) while approaching so that the interaction will be detected at a large tip-sample separation.

3.3 Imaging

3.3.1 Non-Contact Images

Once the sample is approached, we do a series of images to correct any tilt to the sample and to gage the sharpness of the tip. We control the position and bias between sample and cantilever and we measure the frequency shift, dissipation, amplitude, and dc-deflection of the cantilever to either do an $x - y$ plot or spectroscopy on specific regions of the sample. The type of sample and property under investigation will determine whether or not the experiment can be done at liquid helium, liquid nitrogen, or room temperature, as well as at atmospheric pressure or vacuum. Lower temperatures increase the Q of the cantilever and so we have more sensitivity, thermal noise is reduced, and the system is less prone to drift (especially piezo creep). If we are operating the cantilever in FM mode, then we must have a vacuum in order to get a high Q value.

The cantilever is oscillated at its resonance frequency which can change in response to force gradients of the sample. The change in resonance frequency is detected by a PLL or FM demodulator which provides the change in frequency from the original resonance of the cantilever. This signal voltage (proportional to Δf) is compared to the frequency set-point, the difference signal is amplified and applied to the z piezotube so that it can be approached or retracted such that the frequency shift stays at a constant value during the image. The resulting image is essentially the voltage that is sent to the piezotube. Figures 3–2(a) and 3–2(b) are non-contact images taken at liquid nitrogen temperature in a vacuum of self-assembled InAs quatum dots.

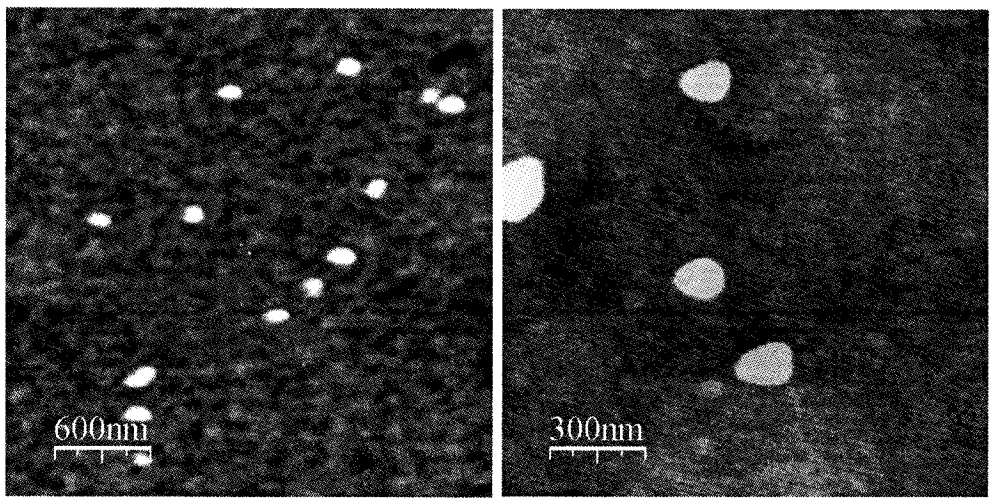

(a) (b)

Figure 3–2: FM mode images of self-assembled InAs quantum dots taken at liquid nitrogen temperature in vacuum. Note the atomic terraces in (b). Image (a) was taken at $V_{Bias} = -0.5\text{V}, \Delta f = -1.1\text{Hz}$, and an oscillation amplitude of 10nm, while (b) was taken with the same oscillation amplitude, at $V_{Bias} = -0.3\text{V}$, and $\Delta f = -1.1\text{Hz}$

3.3.2 Tapping Mode Images with Q-Control

As previously mentioned, tapping mode is a type of AM mode. The cantilever is driven with a constant signal near resonance and increases in tip-sample force cause decreases in the amplitude oscillation due to a greater change in the cantilever's resonance frequency. This decrease can be used as input to a feedback loop for the z piezotube to do images at a constant value of amplitude decrease. The images presented here were done in vacuum and so required a dampening of the intrinsic Q value.

J. Mertz et al. [48] and B. Anczykowski et al. [49] discussed a method somewhere in between the frequency and amplitude modulation modes where the Q of a cantilever can be decreased (Mertz) or increased (Anczykowski) by applying a force proportional to the position of the cantilever, then termed Q_{eff}. An additional feedback loop amplifies and phase shifts the phase-shifted position signal of the cantilever from the photodiode and then sends this signal to the bimorph.

Q-Control allows us to do tapping mode images in the repulsive force regime, often yielding higher resolution of the sample surface, at low temperatures or in vacuums where the intrinsic Q value would normally be too high to stably image in tapping mode (Callahan [50] commented that Q-control could be used to do a tapping mode image in vacuum). By changing the setpoint and phase of the PLL, we can change the apparent Q of the cantilever, in our case we are always wanting to reduce its value to $\sim$500. Figures 3–3(a) and 3–3(b) show how changing the setpoint and phase on the PLL changes the resonance curve of the free cantilever. Figures 3–4(a) and 3–4(b) show some pictures of InAs self-assembled quantum dots taken at

room temperature in vacuum using Q-control. These figures can be compared to the non-contact mode images in 3–2(a) and 3–2(b).

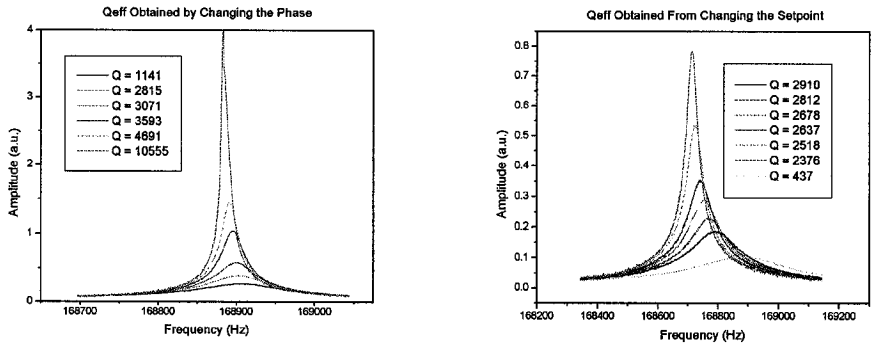

(a) (b)

Figure 3–3: Experimental results showing how changing the phase (a) and the set-point (b) alters the effective Q. Note that there is more control when altering the setpoint as can be expected by looking at Eq. (3.1). These were done at room temperature in a vacuum where the natural Q was 4560.

Since we want to image faster with higher resolution we needed to reduce the Q of our cantilevers to do tapping mode images. According to Rodriguez [51] the equation of motion for the cantilever in the absence of a tip-sample forces is:

$$\mathrm{m}\ddot{\mathrm{z}} + \frac{\mathrm{m}\omega_{\mathrm{o}}}{\mathrm{Q_o}}\dot{\mathrm{z}} + \mathrm{kz} = \mathrm{F_o}\cos(\omega \mathrm{t}) + \mathrm{kG\,z}(\mathrm{t} - \frac{\phi}{\omega}) \tag{3.1}$$

Comparing to Eq. (2.4), one notes that the second term on the right hand side is a force being applied to the cantilever which is proportional to its phase-shifted position. The factor G is a controllable gain used to adjust the additional force. All other symbols are defined as in Eq. (2.4). Using the approximation that we are only interested in steady state solutions, that is solutions where the amplitude of

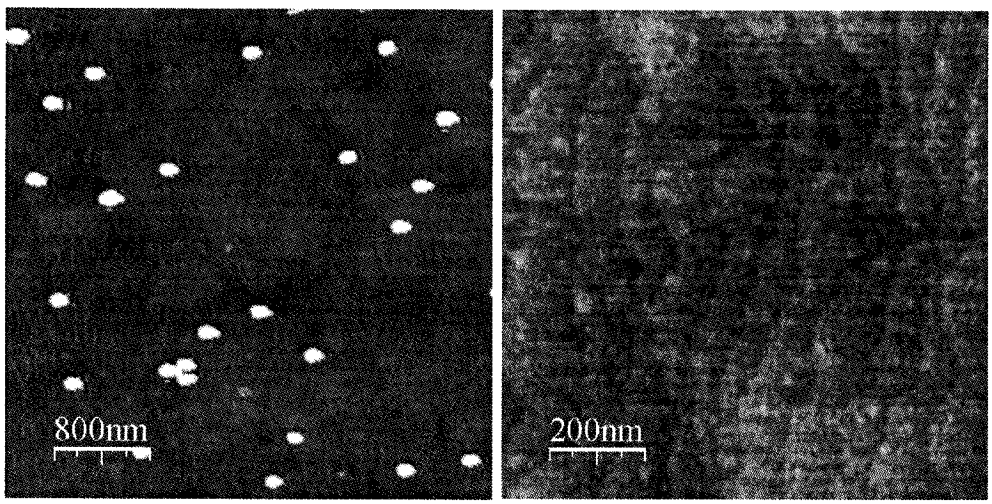

(a) (b)

Figure 3–4: Tapping mode images of self assembled InAs quantum dots taken at room temperature in a vacuum with Q-Control.

the oscillation, A, is not changing with time, then the above can be solved with a general solution $z(t) = z_h(t) + z_p(t)$, where $z_h(t)$ is the solution to the homogenous equation, while $z_p(t)$ is the solution to the particular solution and is given by:

$$\mathrm{z_p(t) = A(\omega, G, \phi)\cos[\omega t - \theta(\omega, G, \phi)]} \tag{3.2}$$

$$\mathrm{A(\omega, G, \phi) = \frac{F_o/m}{\sqrt{\left(\omega_o^2 - \omega^2 + \frac{kG\cos\phi}{m}\right)^2 + \left(\frac{\omega\omega_o}{Q} - \frac{kG\sin\phi}{m}\right)^2}}} \tag{3.3}$$

There are two things to notice, first that this reduces to Eq. (2.5) when G = 0, and secondly that the amplitude of oscillation depends both on the gain and phase difference between the cantilever signal and applied excitation. Since the cantilever oscillates sinusoidally, if $\phi = \pi/2$ then the signal proportional to the position of the cantilever will now be proportional to the velocity of the cantilever, and can cancel

out the damping if G is set to the correct value. In this way the Q_{eff} can be enhanced (which is of great interest to the scientific community for increasing image quality particularly in liquids).

Sulchek et al. [52] used this same method (Q reduction) in conjunction with a new kind of piezotube actuator to create a high-speed tapping mode image with a tip velocity of 2.4 mm/s in air. Their purpose was identical to ours, namely reducing the amount of time required for the cantilever amplitude to change from one steady state to another, i.e. to reduce the transient time. Also worth mentioning are two recent studies done by Tamayo [53] [1] and Hölscher [54][2] .

3.4 Spectroscopy

To do spectroscopy in FM mode the tip-sample gap size, voltage, or both are varied while measuring the cantilever amplitude, resonance frequency shift, and dissipation. Unlike when taking images, the feedback to the piezotube is off so that the cantilever's resonance frequency is not held constant by shifting the position of

[1] the noise of micromechanical oscillators, such as cantilevers, were analyzed when operated under Q control and found that the signal-to-noise ratio is not increased by artificially increasing the Q, but rather remains constant since using the feedback amplifier increases both the thermal noise and the noise coming from the photodiode sensing the cantilever's position.

[2] they found that an enhanced Q actually prevented contact with the sample and the repulsive regime was never reached, however the cantilever resided in a stable position as opposed to normal tapping mode where they found a bistability existed. The result was that for enhanced Q they believed that experimentalists are obtaining better images because the system is more stable.

the sample. Once the feedback is off, either the sample is moved or the bias voltage changed while the response of the cantilever is measured. To avoid destruction of the cantilever tip we set a stopping condition such that if the amplitude drops then the spectroscopy ends. We typically set it to approximately 85-90% of the cantilevers free oscillating amplitude. The data shown in section 4.2 involved changing both the voltage and gap size in order to extract the capacitance of a cantilever tip to fit the result to a model of a spherical capacitor over a plane capacitor. The details of this type of data analysis can be found in Dr. R. Stomp's PhD thesis [41].

CHAPTER 4
Fabrication of High Aspect Ratio Cantilever Tips

The structure of the cantilever, and more importantly the cantilever tip, influences the resolution of the acquired data [55, 56]. As discussed earlier, a theoretical example from Hudlet et al. [33] provides an equation for the force on the tip-apex and tip-cone such that plotting the ratio F_{apex}/F_{total} versus tip-sample gap for various half cone angles (Figure 3–1(b)) emphasizes the effectiveness of reducing the cone angle so that the sample is interacting more with the apex of the tip. A high-aspect ratio tip reduces contributions to the force gradient measurement that originates from the tip's sidewalls [57]. In addition to stray forces from the tip's sidewalls, the tip and sample are often not perpendicular resulting in stray interactions from the sides of the tip (Figure 4–1). The cone angle of the cantilever tip is usually focused on, however one could imagine that this tip-sample misalignment would also affect the resulting force. Although control of the angle α is important, we have noticed that many of the techniques published make it difficult to reproducibly control the final tip angle.

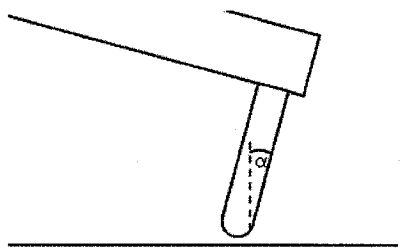

Figure 4–1: Here the cantilever and high aspect ratio tip are on an angle, α with respect to the normal of the sample.

We developed a technique in order to control the radius, length, half cone angle, and angle α of a metallic high aspect ratio cantilever tip. We typically make the tips with an effective radius of curvature of approximately 25 nm, with a length of 20-25 μm, half cone angle $\sim 6°$, and on an angle of $\alpha = 15°$. We have successfully utilized these tips for non-contact AFM and EFM at room temperature, 77 and 4 Kelvin in vacuums of 10^{-4} mbar. It is important that these tips be able to be used down to such low temperatures, yet many of the tips in the literature do not ensure that the construction and conductivity of their tip survives this test. The types of tips described in the following give reproducible results and are easy to construct. Construction of the tips involves the gluing of a 5 μm wire of choice and then using a focused ion beam (FIB) (see the appendix for details on how the FIB works) for shaping the tip [25, 26]. Final tip radii can be less than 5 nm [26], and thus are comparable to carbon nanotube tips, with the entire process taking only a couple of hours. Although gluing a tip to the cantilever is not a new idea it is often not worth the effort compared to using commercially available cantilevers, however our technique can combine any material for the tip with a microfabricated cantilever. Our EFM results show an order of magnitude reduction in the force between tip and sample, and thus background stray capacitance, compared to a commercially available Si cantilever and tip (metallically coated with 100 nm if gold for electrical conductivity). This order of magnitude reduction is desirable for reducing the curvature of the parabolic electrostatic force so that features in the curve are more discernable.

4.1 Fabrication

As in most AFMs, our home built cryogenic AFM has the cantilever on a 15° deviation from the normal of the sample. We thus need to fabricate the tip on a 15° angle from the normal of the cantilever to achieve $\alpha = 0°$. In order to predetermine α we use a FIB (FEI Dual Beam) to cut a guiding slot at an angle of 15° into the cantilever where the metallic wire will be glued (5 nA and 30 kV ion-beam settings). By placing the apex of the triangular cut near the middle of the existing silicon tip there will be added stability for the attached wire, however this is not necessary. A sufficient width for the cut pattern will cause the inside of the slot to fall out with normal handling, whereas if the cuts are too thin then the inside material will stick electrostatically to the cantilever and its removal will require an extra step. One can remedy this situation by pushing out the material with a stiff wire (diameter $15\mu m$) which is securely attached to a micromanipulator. An effective technique for cutting the slot is to first mill most of the triangle (Figure 4–2) and, once this has cut through, follow by milling the two sides furthest from the apex. Cutting of the slot takes about 15 minutes. Figure 4–3(a) shows a normal cantilever tip, and Figure 4–3(b) shows what the cantilever looks like after the triangular slot is removed.

Two micromanipulator stages were fastened perpendicularly to each other onto an L-shaped aluminum support as shown in Figure 4–4. The upper stage moved only in the z-direction and was used to approach the cantilever first to a glue droplet and then to the wire. The glue and wire rested on a glass slide on top of a lower $x-y$ stage. The cantilever was held onto the upper stage by a CuBe spring attached

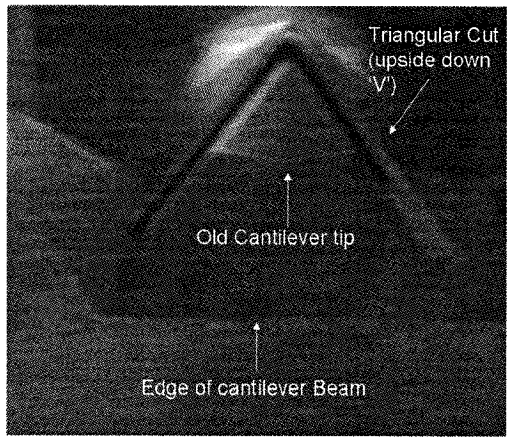

Figure 4–2: FIB Picture of Cutting a Triangular Slot in a Cantilever

to a small shaped aluminum piece that tilted the cantilever at 15°. The aluminum cantilever holder was held onto the stage with a SmCo magnet which had a sufficiently high curie temperature to withstand the heating of the aluminum cantilever holder, required to dry the conductive silver epoxy (EPO-TEK H20E) used to attach the wire.

We cut a 5 μm diameter PtIr wire using a razor blade to a length of $\sim$1 mm using a stereo microscope, and then slid the wire over a groove in a glass slide. To attach the wire, the slot of the cantilever was dipped in a small drop of silver epoxy and then positioned so that it straddled the wire overtop of the groove, thereby preventing the cantilever from being glued to the glass side. If the wire was misaligned, moving the x-y stage proved very effective in positioning the wire into the proper orientation as the sides of the cantilever slot could slightly rotate the wire. A 200 Ω resistor, glued onto the side of the Al cantilever holder, had approximately 20 V applied to it for about one hour in order to heat and consequently cure the epoxy. This stable setup

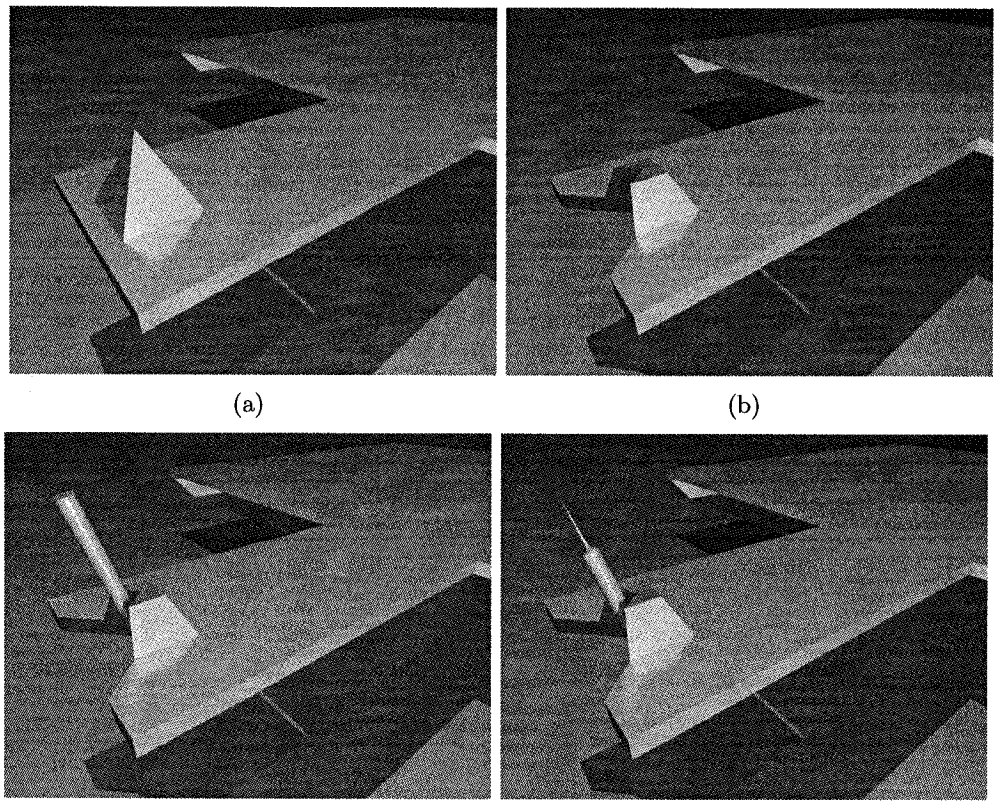

Figure 4–3: Schematic images showing the entire process of making a high aspect ratio tip (not to scale). First, the untouched cantilever is shown (a), next a triangular slot is cut into the cantilever (b). The wire is then glued into the slot and taken to the FIB to be trimmed along its backside and at a certain height above the surface (c), and finally the wire is shaped into a high aspect ratio tip (d).

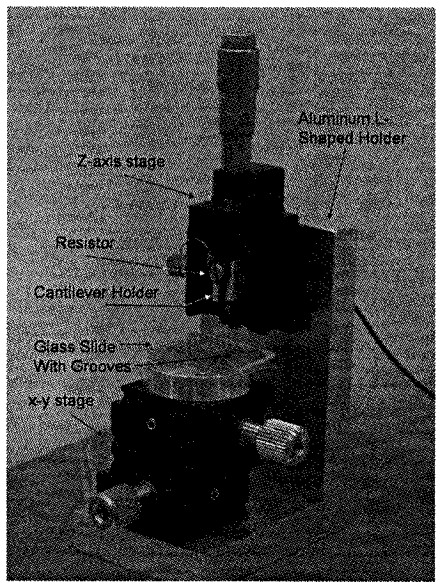

Figure 4–4: Two micromanipulator stages were used to precisely align the slot in the cantilever beam with the cut 5μm wire.

does not require any supervision while the glue is drying. Due to the immobilization of the wire by the glass slide and precut slot of the cantilever, a predetermined angle α is highly reproducible. If starting with an uncoated cantilever a conductive layer would be deposited at this stage. Usually, however, we used coated cantilevers and found that the damage caused to the coating from the FIB is minimal because the glue covers the area of damage.

Finally the cantilevers with glued wires returned to the FIB. The wire was first cut flush along the backside of the cantilever and roughly 50μm from the surface of the cantilever as shown in Figure 4–3(c). The wire was then milled further to fabricate the desired tip shape using the technique reported in [25] and [26]. The shaping technique uses the FIB to successively mill smaller and smaller donut shaped

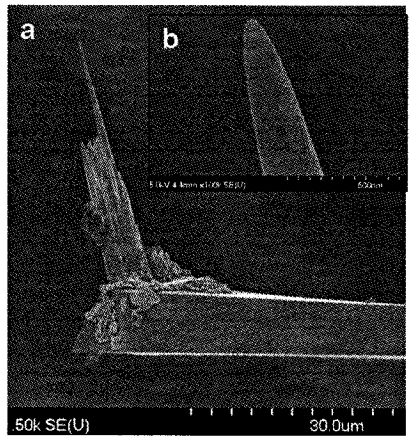

Figure 4–5: SEM Image of High Aspect Ratio Tip. A close up of the apex of the tip is shown in the inset.

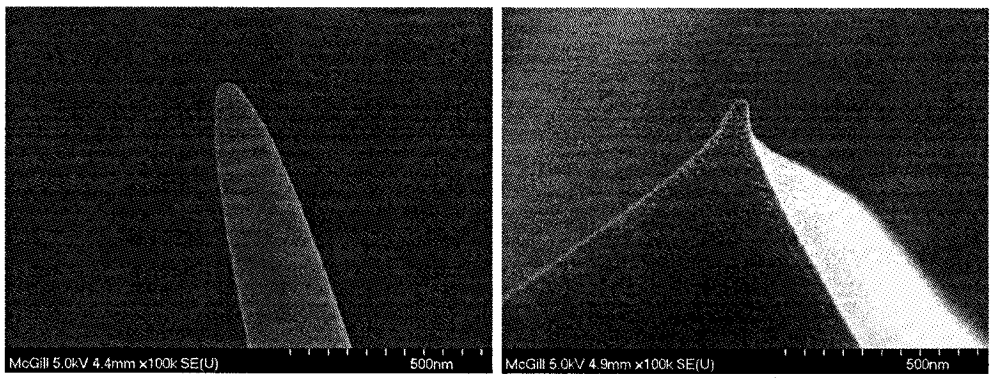

(a) (b)

Figure 4–6: Close up of the tip shown in Figure 4–5 compared to a commercially available tip that has been sputter coated with 10nm Ti and 10nm of Pt.

patterns around the wire and usually takes less than one hour. Figures 4–3(d) and 4–5 shows the final cantilever and tip, while Figures 4–6(a) and 4–6(b) compare a high aspect ratio tip to a commercially available cantilever tip that has been coated with 10 nm of Ti and 10 nm of Pt. We find that this approach allows a very reproducible fabrication of metallic tips at predetermined angles α and radii as well as aspect ratio determined by the FIB processing.

4.2 Results

In the results that follow, frequency-shift was converted to force according to Sader's method [58]:

$$\mathrm{F(z)} = 2\mathrm{k}\int_{\mathrm{z}}^{\infty}\left(1+\frac{\mathrm{a}^{1/2}}{8\sqrt{\pi(\mathrm{t}-\mathrm{z})}}\right)\Omega(\mathrm{t})-\frac{\mathrm{a}^{3/2}}{\sqrt{2(\mathrm{t}-\mathrm{z})}}\frac{\mathrm{d}\Omega(\mathrm{t})}{\mathrm{dt}}\mathrm{dt} \qquad (4.1)$$

where $\Omega(z) = \Delta\omega(z)/\omega_{res}$, which is the ratio of the frequency shift ($\Delta\omega$) to the resonance frequency (ω_{res}), a is the amplitude of oscillation, k is the spring constant, z is the tip-sample distance, and t is an integration variable. This conversion can be used for all oscillation amplitudes of the cantilever. Calculation of the capacitance of the cantilever was done using a method where the frequency shift data is collected as the tip-sample distance is changed for a number of voltages and then the information is stored in a matrix so that it can be plotted in the way shown in Figure 4–7.

The described cantilevers and tips have been used down to temperatures as low as 4 K where their conductivity was verified by the parabolic background that was detected through a force voltage measurement. Data over a gold sample shows

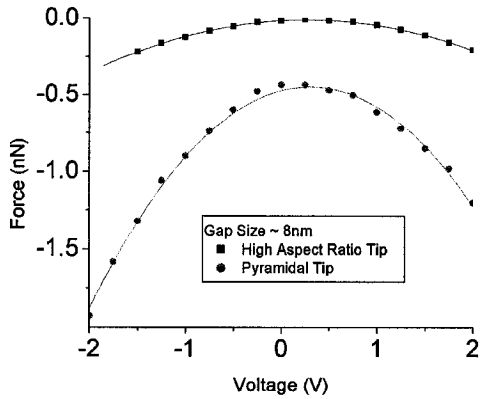

Figure 4–7: Force vs Voltage curves for a high aspect ratio tip and commercially available tip coated with 100nm gold over a gold sample. The high aspect ratio tip gives a reduction in the curvature as well as the offset of the parabola due to smaller van der Waals interactions. Notice the difference in V_{CPD} (the position of the minimum in the parabola) for the two tips, one Au and one PtIr, over the gold sample. Note also that the the pyramidal tip does not fit the parabola as well as the high-aspect ratio tip because data taken closer to the sample (8nm) were displayed in order to show some curvature in the high-aspect ratio tip data, but as the tip approaches the sample forces other than the electrostatic force become more noticeable as a deviation from the parabolic shape. Data for the pyramidal tip was collected by Dr. R. Stomp [41]

that the measured force is approximately one order of magnitude less than the measurements using a commercially available Si cantilever that has been coated with a metallic layer. These results, plotted in Figure 4–7, show that the high aspect ratio tip gives a substantial reduction in curvature of the parabolic background due to the reduction of capacitive interactions with the shank of the tip. The higher aspect ratio tip also interacts much less with forces other than the electrostatic variety resulting in a strongly reduced offset of the parabola due to other interactions (such as vdW). In terms of the general properties of these cantilevers, we found the resonance frequency and Q factor to be within the range of the commercially available cantilever.

The deviation of the angle α from the expected value was small (less than 0.5^o for a batch of $\sim$10 tips fabricated this way). Since α is determined by the cuts made by the FIB, the two sources of deviation could come from a misaligned FIB beam or the flatness of the cantilever with respect to the carbon tape used for mounting in the FIB.

One notable property of these tips is that they are reusable. Not only do we use cantilevers with previously damaged tips, but if the high-aspect ratio tip is damaged during an experiment it can be taken back to the FIB for reshaping.

An interesting way to correlate the results obtained from these tips is to extract the capacitance from the force - voltage cures. By fitting a parabola to the curves in Figure 4–7, one can get a value for the curvature of the parabola which is the change in capacitance with respect to tip-sample distance, $\partial C/\partial z$. This value can be fitted to the derivative of a sphere-plane capacitor system, for example Hudlet et al. [33]

give:

$$C(z) = 2\pi\epsilon_o R \ln(1 + \frac{R}{z}) \tag{4.2}$$

C is the capacitance, ϵ_o is the permittivity of free space, and R is the radius of the spherical tip. Figure 4–8 is a fit to the derivative of Eq. (4.2) where the radius of the tip is best modeled as 24.7 nm which agrees very well with the SEM images of such tips (Figure 4–6(a)). Then it is easy to fit the data to Eq. (4.2) as shown in Figure 4–9 by adding an integration constant.

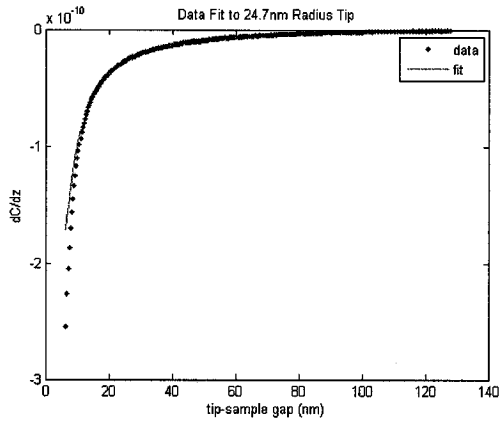

Figure 4–8: Experimental data using a high-aspect ratio tip is fit to the derivative of Eq. (4.2) to determine the radius of the tip, here 24.7 nm provides the best fit.

It is interesting that the data for this tip follows the sphere-plane model over such a large range. To show why, Figure 4–10 was included from [41] which plots the capacitance and its first derivative (with respect to tip-sample distance) for a 100 nm thick gold coated commercial Si cantilever tip over a gold surface. Note that the plot for the capacitance looks different than in Figure 4–9 because it is a log-log plot. This tip, which was in no means a high aspect ratio tip, does not follow the

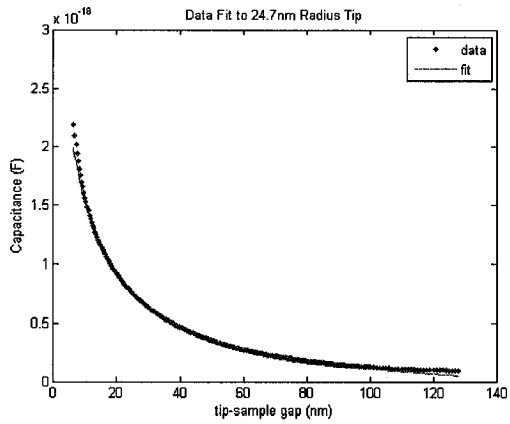

Figure 4–9: Capacitance of sphere-plane for a sphere of radius 24.7nm fit to experimental data that is shifted to account for the integration constant.

sphere-plane model for nearly as large of distance. As explained previously, at larger distances the geometry of the tip begins to contribute which can be significant if the geometry of the tip is much larger than the tip apex. However, as the high aspect ratio tip follows the sphere-plane capacitance model over such a large distance, the force on the tip apex must be a greater portion of the total force, as was expected.

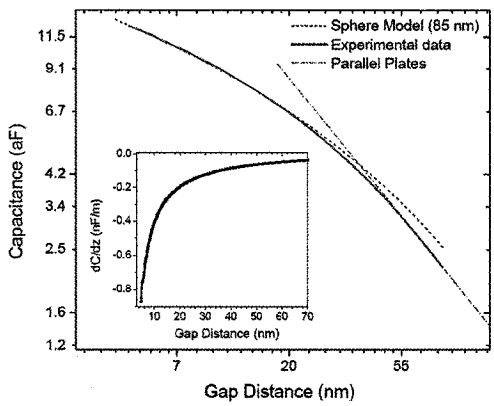

Figure 4–10: Capacitance of a gold coated (100 nm thick coating) Si cantilever tip over a gold surface. Experimental data is compared to a sphere-plane and plane-plane capacitive plate model. The first derivative of the capacitance is in the inset. Graph taken from [41]

CHAPTER 5
Conclusion and Outlook

This thesis demonstrated the realization of both a $x-y$ sample walker with a capacitive sensor for use in a low temperature AFM, and the fabrication of high-aspect ratio metallic cantilever tips for use in non-contact AFM where the tip radius, cone angle, height, and tip angle are controlled. Both will be used in future experiments. In particular, the new tips will be used in the very near future for investigating the properties of electrons tunneling into Quantum Dots (QD).

QDs are small structures, typically a few tens of nanometers high and wide, and so possess quantum properties such as discrete energy levels. For this reason they are sometimes called 'artificial atoms'. Previously, work was done in our group to investigate the properties of QDs, where a conductive AFM tip was positioned above a QD and a sweep in the bias voltage revealed changes in frequency shift (in non-contact mode) and dissipation resulting from electrons tunneling into the surface. The complete analysis of these results are available in [41].

Our microscope has gone through a lot of repairs to get it working well at liquid helium temperature and we recently obtained a number of new samples from The National Research Council in Ottawa, Canada, some the same as, and some with different properties to, the ones analyzed in [41]. As of yet we have only looked at a sample consisting of self-assembled InAs QDs which are situated 20nm above a 2D electron gas (2DEG) where the two layers are separated by a tunneling barrier. Topographic images of the sample were previously shown, but are shown again in Figures 5–1(a) and 5–1(b) in 3D. As proof-of-principle, we tried the same experiments

that yielded single electron charging events as reported in [15], and obtained a similar spectra as shown in Figure 5–2.

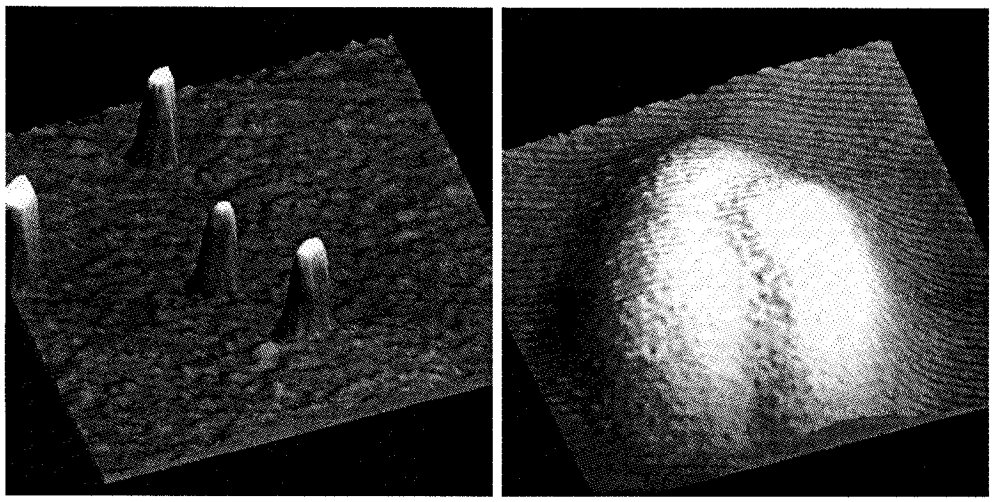

(a) (b)

Figure 5–1: Images of Self-Assembled QDs taken at liquid nitrogen temperature in non-contact mode. The left image is $1.5\mu m^2$ of four QDs and the right $150nm^2$ of one QD.

This data was taken using a commercially available cantilever from Nanosensors which was coated with 10 nm Ti and 10 nm Pt. The tip of a similar cantilever is shown in Figure 4–6(b). The high-aspect ratio tips made with the FIB should, for reasons explained in chapter 4, reduce the curvature of the parabolic background of the frequency shift vs voltage spectroscopy in order to make the jumps in frequency shift more apparent. In fact, this was the original motivation for this work.

Future experiments will also investigate how changes in the frequency shift and dissipation are affected with different sized tunneling barriers and with capped QDs (which are being investigated for QD lasers).

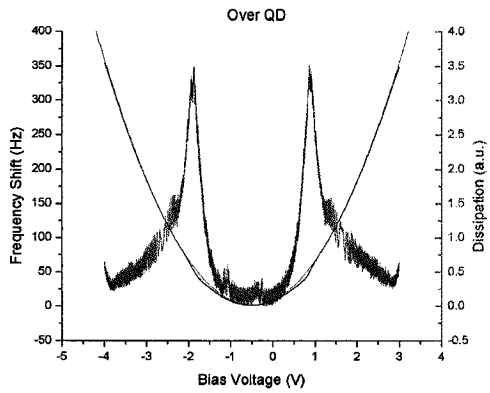

Figure 5–2: The recorded frequency shift and dissipation of the cantilever as the voltage is swept for the cantilever being held over a quantum dot situated above a 2DEG. The blue curve is a parabolic fit to the frequency shift. Notice the jumps in frequency shift that correspond to peaks in the dissipation which is believed to be caused by electrons tunneling into the QD from the 2DEG.

Appendix: How the FIB Works with Application to Creating High Aspect Ratio Cantilever Tips

To shape the high aspect ratio tips for electrostatic force microscopy, the FEI Dual-Beam focused ion beam (FIB) and scanning electron microscope (SEM) at Ecole Polytechnique, at the University of Montreal were used. The focused ion beam is created from a liquid gallium metal ion source which is focused using a two-lens focusing column [59]. The user sets the beam energy and size with which the ions bombard the sample to mill out specific regions. The patterns for milling are drawn directly on an ion beam image. The process can be automated using predesigned pixel instructions, however this is not feasible for the fabrication of the tips described in chapter 4 because they are such small and tall structures that one has to hunt down places where additional milling may be required, in addition the sample may drift due to charging. Figure 5–3 depicts how the instrument has the ion and electron source offset by 52° from each other. If you choose your angles carefully you can watch what you are milling in 'real time' as electron beam images can be taken while milling. The electron beam can also be used to neutralize your sample while milling if charging is a problem.

This system also has gas injection and deposition capabilities. Gas injection can reduce the amount of redeposition onto the sample surface as well as reduce milling times (an interesting paper on the topic from Santschi et al. [60]). Deposition of various materials have a number of applications, even some for making different types of cantilever tips. We did not require these features for creating high aspect

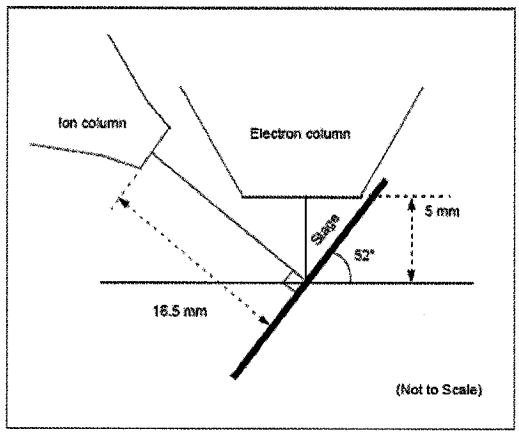

Figure 5–3: The focused ion beam and electron beam are separated by a 52° angle. [59]

ratio tips because there is not a significant amount of redeposition onto the cantilever after milling the wire because it is so tall. There is, however, significant deposition after cutting the slot into the tip, but this is covered with the silver epoxy and so does not influence further steps in the fabrication process. We chose not to use the deposited materials because their conductivity was not easily determined, especially at low temperatures (4 K) where our cantilevers would be used.

In order to minimize charging the cantilevers are mounted on carbon tape and the additional precaution of covering them with copper tape can be used but is usually not necessary. It takes some experience to set up the SEM and FIB system, for example it is very convenient to have the FIB and SEM beams coincide. A convenient method for milling a cantilever is to use the Dynamic Drift Control option, where a small marker on an unused area of the cantilever serves to correct for the drift in the patterning. Without dynamic drift control, the pattern would have to

be readjusted approximately every four minutes to correct the drift. The triangular slot, or 'V' slot, is cut in two installments where initially almost all of the slot is cut except for two small portions of the upper part of the 'V'. Once this section has been cut through, the remaining part of the 'V' is cut. This process keeps the cut out region from moving around (due to charging) which can block the FIB, leading to longer milling times. One precaution that we need to take is to prevent the milling of the cantilever's conductive coating as much as possible. To achieve this, we use small beam currents and few snapshots when imaging the cantilever. To cut the slot into the cantilever a beam current of 5000 pA and beam energy of 30kV is used.

To shape the end of the cantilever tip, a series of donut cuts are made around the wire. To get an idea of a typical fabrication process see table 5-1 where the two steps involving a variable length of time are when additional pieces of material that needed removal are hunted down and milled away. Since it is often difficult to see them in the FIB image, it can sometimes take a long time. This cautious approach prevents accidental milling through of the cantilever, thereby compromising the integrity of the glued wire.

Table 5–1: Tip Shaping Process Flow

Step	Ion Beam Current (pA)	Outer Radius (nm)	Inner Radius (nm)	Time (min)
1	500	3	1.5	3
2	500	-	-	variable
3	500	1.75	0.75	2.5
4	500	-	-	variable
5	100	1.5	0.5	3.5
6	100	0.9	0.4	1.5
7	100	0.8	0.25	1

References

[1] G. Binnig, H.Rohrer, Ch.Gerber, and E.Weibel, Phys. Rev. Lett. **49**, 57 (1982).

[2] G. Binnig, C. Quate, and Ch.Gerber, Phys. Rev. Lett. **56**, 930 (1986).

[3] F. Giessibl, Rev. Mod. Phys. **75**, 949 (2003).

[4] Y. Sugimoto et al., Phys. Rev. B **73** (2006).

[5] W. Muller et al., Science **268**, 272 (1995).

[6] L. Blasdel, S. Banerjee, and S. Wong, Science **268**, 272 (1995).

[7] V. Zorbas et al., Chem. Commun. , 4598 (2006).

[8] F. Kersey, W. Yount, and S. Craig, J. Am. Chem. Soc. **128**, 3886 (2006).

[9] N. Oyabu, O. Custance, I. Yi, Y. Sugawara, and S. Morita, Phys. Rev. Lett. **90** (2003).

[10] J. E. Stern, B. D. Terris, H. J. Mamin, and D. Rugar, Appl. Phys. Lett. **53**, 2717 (1988).

[11] C. Schonenberger and S. F. Alvarado, Phys. Rev. Lett. **65**, 3162 (1990).

[12] L. J. Klein and C. C. Williams, Appl. Phys. Lett. **79**, 1828 (2001).

[13] L. J. Klein and C. C. Williams, Appl. Phys. Lett. **81**, 4589 (2002).

[14] A. Dana and Y. Yamamoto, Nanotechnology **16**, S125 (2005).

[15] R. Stomp et al., Phys. Rev. Lett. **94** (2005).

[16] D. Rugar, R. Budakian, H. Mamin, and B. Chui, Nature **430**, 329 (2004).

[17] G. Schitter, P. Menold, H. Knapp, F. Allgower, and A. Stemmer, Rev. Sci. Instrum. **72**, 3320 (2006).

[18] G. Schitter, R. Stark, and A.Stemmer, Ultramicroscopy **100**, 253 (2006).

[19] H. Dai, J. Hafner, A. Rinzler, D. Colbert, and R. Smalley, Nature **384**, 147 (1996).

[20] S. S. Wong, J. D. Harper, P. T. Lansbury, and C. M. Lieber, Journal of the American Chemical Society **120**, 603 (1998).

[21] C. Cheung, J. Hafner, and C. Liber, PNAS **97**, 3809 (2000).

[22] J. Hafner, C. Cheung, T. Oosterkamp, and C. Liber, J. Phys. Chem. B **105**, 743 (2001).

[23] D. Biegelsen, F. Ponce, J. Tramontana, and S. Koch, Appl. Phys. Lett. **50**, 696 (1987).

[24] D. Biegelsen, F. Ponce, and J. Tramontana, Appl. Phys. Lett. **54**, 1223 (1989).

[25] M. Vasile, D. Grigg, J. Griffith, E. Fitzgerald, and P. Russell, Rev. Sci. Instrum. **62**, 2167 (1991).

[26] K. Akiyama et al., Rev. Sci. Instrum. **76** (2005).

[27] C. Menozzi, G. C. Gazzadi, A. Alessandrini, and P. Facci, Ultramicroscopy **104**, 220 (2005).

[28] P. Pingue et al., Appl. Phys. Lett. **88**, 043510 (2006).

[29] J. N. Israelachvili, *Intermolecular and Surface Forces with Applications to Colloidal and Biological Systems*, Academic Press, 1985.

[30] J. Hutter and J. Bechhiefer, J. Appl. Phys. **73**, 4123 (1993).

[31] U. Hartmann, J. Vac. Sci. Technol. B **9**, 465 (1991).

[32] L. Kantorovich, A. Livshits, and M. Stoneham, J. Phys.:Condens. Matter **12**, 795 (2000).

[33] S. Hudlet, M. S. Jean, C. Guthmann, and J.Berger, Eur. Phys. J. B **2**, 5 (1998).

[34] D. Sarid, *Scanning Force Microscopy with Applications to Electric, Magnetic and Atomic Forces*, Oxford University Press, 1994.

[35] Y. Martin, C. Williams, and H. Wickramasinghe, J. Appl. Phys. **61**, 4723 (1987).

[36] T. Albrecht, P.Grutter, D. Horne, and D.Rugar, J. Appl. Phys. **69**, 668 (1991).

[37] Nanosurf, *easyPLL FM Sensor Controller*, 2 edition.

[38] M. Roseman, Design and characteristics of a low temperature atomic force microscope, Master's thesis, McGill University, 1997.

[39] M. Roseman, *Low Temperature Magnetic Force Microscopy Studies of Superconducting Niobium Films*, PhD thesis, McGill University, 2001.

[40] M. Roseman and P. Grutter, Rev. Sci. Instrum. **71**, 3782 (2000).

[41] R. Stomp, *Dissipative and Electrostatic Force Spectroscopy of InAs Quantum Dots by Non-contact Atomic Force Microscopy*, PhD thesis, McGill University, 2005.

[42] D. Rugar, H. Mamin, and P.Guethner, Appl. Phys. Lett. **55**, 2588 (1989).

[43] T. Albrecht, P. Grutter, D.Rugar, and D. Smith, Ultramicroscopy **42–44**, 1638 (1992).

[44] S. Field and J. Barentine, Rev. Sci. Instrum. **71**, 2603 (2000).

[45] K. Bruland et al., Rev. Sci. Instrum. **70**, 3542 (1999).

[46] J. Zhu, M. Brink, and P. L. McEuen, Appl. Phys. Lett. **87** (2005).

[47] P. Fallahi et al., Nano Lett. **5**, 223 (2005).

[48] J. Mertz, O. Marti, and J. Mlynek, Appl. Phys. Lett. **62**, 2344 (1993).

[49] B. Anczykowski, J. Cleveland, D. Kruger, V. Elings, and H.Fuchs, Appl. Phys. A **66**, S885 (1998).

[50] F. Callaghan, X.Yu, and C. Mellor, Appl. Phys. Lett. **81**, 916 (2002).

[51] T. Rodriguez and R.Garcia, Appl. Phys. Lett. **82**, 4821 (2003).

[52] T. Sulchek, M. Jenke, P. Hoffmann, and J.Brugger, Appl. Phys. Lett. **76**, 1473 (2000).

[53] J. Tamayo, J. Appl. Phys. **97**, 044903 (2005).

[54] H. Hoscher, D. Ebeling, and U. Schwarz, J. Appl. Phys. **99**, 084311 (2006).

[55] S. Belaidi, P. Girard, and G. Leveque, J. Appl. Phys. **81**, 1023 (1997).

[56] S. Belaidi, P. Girard, and G. Leveque, Microelectronics and Reliability **37**, 1627 (1997).

[57] R. Stomp, Y. Miyahara, D. Weiner, and P. Grutter, Measuring absolute tip-sample capacitance with an atomic force microscope.

[58] J. Sader and S. Jarvis, Appl. Phys. Lett. **84**, 1801 (2004).

[59] F. Company, *FEI DB 235 Manual*, 2003.

[60] C. Santschi, M. Jenke, P. Hoffmann, and J. Brugger, Nanotechnoloy **17**, 2722 (2006).